mater.scichina.com link.springer.com

Published online 7 July 2021 | https://doi.org/10.1007/s40843-021-1698-3
Sci China Mater 2021, 64(12): 3027–3036

Ultrawide-bandgap (6.14 eV) $(AlGa)_2O_3/Ga_2O_3$ heterostructure designed by lattice matching strategy for highly sensitive vacuum ultraviolet photodetection

Yuqiang Li, Dan Zhang*, Lemin Jia, Siqi Zhu, Yanming Zhu, Wei Zheng* and Feng Huang

ABSTRACT One judiciously designed strategy of utilizing an ultrathin but conductive Ga_2O_3:Si nanolayer to prepare $(AlGa)_2O_3$ crystalline film is demonstrated. Benefiting from the existence of Ga_2O_3:Si nanolayer, a high-quality $(Al_{0.68}Ga_{0.32})_2O_3$ sesquioxide film with 68 at.% aluminum was epitaxially grown on sapphire substrates, which was characterized by high-resolution transmission electron microscopy, X-ray photoelectron spectroscopy and X-ray diffraction. Its bandgap was broadened to 6.14 eV, and a vacuum ultraviolet (VUV) $(AlGa)_2O_3/Ga_2O_3$:Si photodetector was subsequently fabricated. The detector exhibits a pretty high on-off ratio of about 10^3, an open-circuit voltage of 1.0 V and a responsivity of 8.1 mA W^{-1} at 0 V bias voltage. The performances imply that the proposed strategy is valuable for improving the quality and also adjusting the bandgap of $(AlGa)_2O_3$ sesquioxides, which is expected to facilitate their application in VUV photodetection.

Keywords: $(AlGa)_2O_3$, ultrawide bandgap, vacuum ultraviolet, photovoltaic detector

INTRODUCTION

Vacuum ultraviolet (VUV) photodetectors own great application prospects in space science, based on their ability to identify the radiation less than 200 nm [1–5]. In order to conduct efficient monitoring, the characteristics like small size and low power consumption, as well as the performance including high sensitivity, large switching ratio and good stability [6–8], are pursued. Compared with photoconductive detectors, photovoltaic ones possess faster speed and easier integration and have the ability to operate without bias voltage, making them a preferred geometric structure for VUV detectors [9–11].

In recent years, the mainly used materials for preparing VUV detectors are those naturally ultrawide-bandgap semiconductor materials such as AlN [12–14], AlGaN [15–17] and BN [18–22]. Gallium oxide (Ga_2O_3) is also considered to be a candidate for VUV detection, by adding aluminum component to obtain $(AlGa)_2O_3$ ternary sesquioxides with a freely-adjustable bandgap (4.9–8.8 eV). Besides, it possesses the controllable carrier concentration [23–26]. Although there have been various reported methods for growing $(AlGa)_2O_3$ alloy, effective usage of a high aluminum content (Al > 60 at.%) is indeed desired for broadening the bandgap of $(AlGa)_2O_3$ sesquioxides to VUV region (> 6 eV) [27–30]. However, limited by the compatibility with substrate materials, the increase of aluminum content usually causes $(AlGa)_2O_3$ sesquioxides to transform into amorphous phase, which hampers the preparation of high-performance VUV detectors. Sapphire as a kind of commercial large-size single-crystal substrate is often used for the growth of $(AlGa)_2O_3$ owing to the small lattice mismatch between them [31,32].

However, $(AlGa)_2O_3$ detectors with high aluminum contents are still constrained within planar photoconductive types, because the sapphire substrates are not conductive for transmitting carriers [27–29]. To address this challenge, we propose an method of inserting an conductive ultrathin Ga_2O_3:Si film (~10 nm) into the interface between sapphire and ternary compounds, to construct a highly sensitive photovoltaic $(AlGa)_2O_3$ VUV detector. The lattice mismatch between $(AlGa)_2O_3$ and sapphire is almost not affected by a 10-nm inserted nanolayer, ensuring the crystalline quality of the $(AlGa)_2O_3$ epitaxial film (Supplementary information (S1)). In addition, the conductive Ga_2O_3:Si film will generate a built-in electric field, enabling the detector to work without an external bias voltage.

In this work, metal organic chemical vapor deposition

State Key Laboratory of Optoelectronic Materials and Technologies, School of Materials, Sun Yat-sen University, Guangzhou 510275, China
* Corresponding authors (emails: zhangdan8@mail.sysu.edu.cn (Zhang D); zhengw37@mail.sysu.edu.cn (Zheng W))

 © Science China Press and Springer-Verlag GmbH Germany, part of Springer Nature 2021

(MOCVD) method was used to deposit an ultrathin Ga_2O_3:Si film on the sapphire substrate as a conductive layer. The $(Al_{0.68}Ga_{0.32})_2O_3$ sesquioxide film was further epitaxially grown on the Ga_2O_3:Si layer, possessing a broadened bandgap of 6.14 eV. Based on the heterostructure, an $(Al_{0.68}Ga_{0.32})_2O_3/Ga_2O_3$:Si/sapphire photovoltaic VUV detector with a spectral response was prepared, and the device exhibited a high on-off ratio over 10^3, a responsivity of 8 mA W^{-1} at 0 V bias and a fall time of 0.2 s. The strategy of constructing fully gallium oxide homogeneous photovoltaic detectors with a conductive nanolayer may enlighten the research of using other semiconductor materials for optical and photoelectronic devices.

EXPERIMENTAL SECTION

Film growth

A 10-nm-thick Ga_2O_3:Si film was deposited on *c*-plane sapphire substrates by the MOCVD method, and a $(Al_{0.68}Ga_{0.32})_2O_3$ film was deposited on the Ga_2O_3:Si layer subsequently. During the film growth, the substrate temperature was maintained at 800°C, and the pressure in the reaction chamber was maintained at 250 torr (1 torr=1.33322×10^2 Pa). N_2O, SiH_4, trimethyl-Al (TMA) and triethyl-gallium (TEGa) were used as precursors for the film growth.

Materials characterization

The cross-sectional morphology, high-resolution transmission electron microscopy (HRTEM) and element line scan of the film were characterized by Tecnai G2 F30 of FEI (300 kV). X-ray photoelectron spectroscopy (XPS) characterization was performed by Thermo Fisher ESCALAB 250Xi. The X-ray diffraction (XRD) and ultraviolet-visible absorption and transmission spectra of the film were tested by PANalytical X-ray diffractometer and Shimadzu UV-3600 spectrophotometer, respectively.

Device fabrication

A circular platinum metal layer with a radius of 200 μm and a thickness of about 20 nm was deposited on the surface of $(Al_{0.68}Ga_{0.32})_2O_3$ as the positive electrode by using physical mask and ion sputtering. Thermally fused metal indium was connected with Ga_2O_3:Si as a negative electrode.

Device characterization

The device was tested on a SEMISHARE SE-4 probe station. The *I*-*V* characteristics of the detector and the conductivity of the metal electrodes were characterized by a KEITHLEY 2636B source meter. The 185-nm light was produced by a low-pressure mercury lamp. The illumination intensity was adjusted by changing the position of the mercury lamp, and the light power was measured by the VXUV20A photodetector of Opto Diode Corp. The spectral responsivity was measured by using a self-assembled system, with Shimadzu UV-2600 as the light source and KEITHLEY 2636B as the sourcemeter.

RESULTS AND DISCUSSION

Fig. 1a and b show a schematic diagram of the preparation process of the $(Al_{0.68}Ga_{0.32})_2O_3/Ga_2O_3$:Si/sapphire heterojunction. The MOCVD method was used to deposit a Si-doped gallium oxide film on sapphire substrates. In order to reduce pre-reaction, inert (low chemically active) N_2O gas was used as the precursor [33]. Considering that high-quality conductive gallium oxide film does not require excessive Si doping, the large-flow carrier gas was adopted for transporting silane to reduce the Si element concentration. TMA with a higher chemical activity was chosen to react with N_2O to grow $(Al_{0.68}Ga_{0.32})_2O_3$, ensuring the incorporation of high-content Al.

Fig. 1c shows the lattice structure of β-phase $(AlGa)_2O_3$, in which O_2, O_7 and O_{12} oxygen atoms are distributed on $(\bar{2}01)$ equivalent plane of $(AlGa)_2O_3$. When the gallium oxide film grows along the $(\bar{2}01)$ plane, the Ga atoms combine with the O atoms in sapphire *c*-plane (O_{sa}) or the O atoms in gallium oxide $(\bar{2}01)$ plane (O_{ga}) in the same way [34]. Therefore, the mismatch between O_{sa} and O_{ga} can be analyzed by comparing the length of O_{sa}–O_{sa} and O_{ga}–O_{ga} in the two crystal planes as changed with the Al content. Through the first principle calculation, the atomic distances between O_7 and O_7 (d_{7-7}) and the distances between O_7 and O_{12} (d_{7-12}) in different Al content situations are obtained, as shown in Fig. 1d. The lengths of O_{ga}–O_{ga} (namely d_{7-7} and d_{7-12}) decrease gradually with the increase of Al content, which is closer to the O_{sa}–O_{sa} length (around 2.87 Å) in the *c*-plane of sapphire [34]. The calculation results imply that the mismatch between $(AlGa)_2O_3$ and *c*-plane sapphire substrate decreases with the increasing Al content. In other words, sapphire substrate is beneficial to growing $(AlGa)_2O_3$ film with high Al contents.

It can be clearly seen from Fig. 2a that except for the sapphire's (006) peak, only the $(\bar{2}01)$, $(\bar{4}02)$ and $(\bar{6}03)$ characteristic peaks of $(Al_{0.68}Ga_{0.32})_2O_3$ are observed, implying that the sesquioxides belong to the single-oriented crystalline phase [11,35]. The full width at half maxima

© Science China Press and Springer-Verlag GmbH Germany, part of Springer Nature 2021

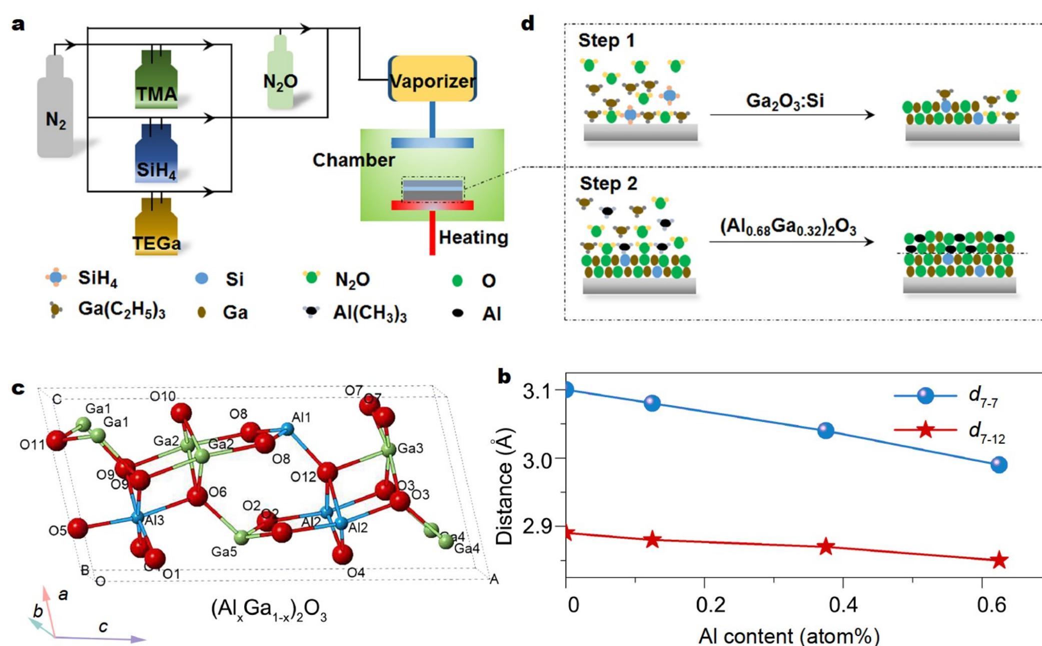

Figure 1 Schematic diagram of film growth and the lattice structure. (a, b) Preparation diagram of $(Al_{0.68}Ga_{0.32})_2O_3/Ga_2O_3$:Si/sapphire heterojunction. The $(Al_{0.68}Ga_{0.32})_2O_3$ and Ga_2O_3:Si films were grown by the MOCVD method. $Al(CH_3)_3$, SiH_4, $Ga(C_2H_5)_3$ and N_2O were used as the precursors, and N_2 was used as the carrier gas. (c) Lattice structure diagram of $(AlGa)_2O_3$. (d) Oxygen atom distances between O_7 and O_7(d_{7-7}) and between O_7 and O_{12} (d_{7-12}) as a function of Al content in the $(AlGa)_2O_3$ system.

(FWHM) of this ($\bar{2}01$) peak is about 0.46°, which indicates the good crystalline quality. According to the relationship between absorption coefficient and semiconductor bandgap (Fig. 2b), the optical bandgap of the film is estimated to be around 6.14 eV, which meets the requirement of VUV detection. This result is also consistent with the bandgap value of 6.1 eV obtained by XPS calibration of O 1s energy level (Fig. 3f) [36], further confirming the credibility of bandgap measurement. Fig. 2c shows the cross-sectional morphology of the dense epitaxial $(Al_{0.68}Ga_{0.32})_2O_3/Ga_2O_3$:Si film on a sapphire substrate, and a thickness of ~134 nm is observed.

Fig. 2d shows the cross-sectional scanning electron microscopy (SEM) morphology of the heterojunction, in which the boundary between the gallium oxide layer and the sapphire substrate is clearly observed. Fig. 2d_1 is an enlarged TEM view of the selected area at the interface. The top is the image of sapphire lattice and the bottom is that of $(AlGa)_2O_3$. The Ga_2O_3:Si layer is not observed at the interface, because they cannot be distinguished by HRTEM, since the lattice of Ga_2O_3:Si and $(Al_{0.68}Ga_{0.32})_2O_3$ layers are almost the same (Fig. S1). The shadow region at the interface in Fig. 2d_1 is more likely to be caused by the effect of stress on the crystal lattice, which originates from the mismatch between gallium oxide and sapphire [37].

The secondary ion mass spectrometry (SIMS) result supplies the atom ratio of Si/Ga in Ga_2O_3:Si film is around 1/2850 (Fig. 2g). The HRTEM images and selected area electron diffraction (SAED) patterns of sapphire substrates were further analyzed in Fig. 2d–d_1, with the interplanar crystal spacing and crystal indices annotated [38]. The HRTEM image of $(Al_{0.68}Ga_{0.32})_2O_3$ film shows that the grown ternary sesquioxides possess high lattice quality and the atoms are arranged neatly, which indicates that the Al component has been incorporated without disorder. The ($\bar{2}01$) interplanar spacing marked in Fig. 2f is 0.46 nm, which is similar to the lattice constant of gallium oxide reported [37,39]. Because the change of the lattice constant of $(Al_{0.68}Ga_{0.32})_2O_3$ is estimated to be only a few thousandths of a nanometer different from that of Ga_2O_3 by analyzing the XRD peaks with Bragg formula, the tiny distinction cannot be distinguished by HRTEM. More large-scale HRTEM images are placed in Fig. S2. As shown in Fig. 2f_1, the marked crystal indices in SAED pattern of $(Al_{0.68}Ga_{0.32})_2O_3$ are consistent with the XRD characterization results.

The high-resolution XPS spectra of the film (Fig. 3a–c) show accurate element valence states in the $(Al_{0.68}Ga_{0.32})_2O_3$ film [40]. The binding energy of 2p orbital of Al element is around 74.8 eV, indicating that Al^{3+}

 © Science China Press and Springer-Verlag GmbH Germany, part of Springer Nature 2021

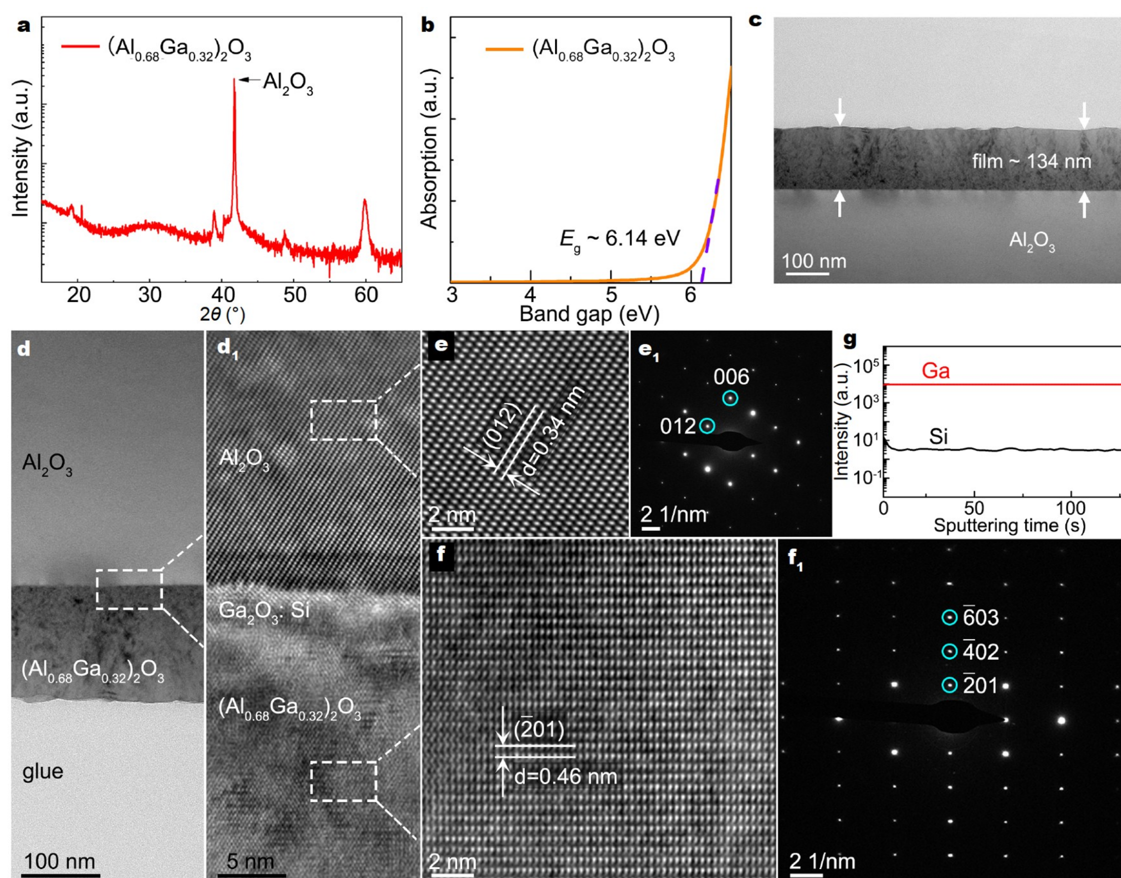

Figure 2 Material characterizations. (a) XRD pattern of the $(Al_{0.68}Ga_{0.32})_2O_3/Ga_2O_3$:Si film as grown by MOCVD. The observed ($\bar{2}$01), ($\bar{4}$02), ($\bar{6}$03) peaks are located at 18.9°, 38.4° and 59°, respectively. (b) Relationship between the bandgap of$(Al_{0.68}Ga_{0.32})_2O_3$ film and incident photon energy. (c) Cross-sectional SEM image of $(Al_{0.68}Ga_{0.32})_2O_3/Ga_2O_3$:Si/sapphire heterojunction. (d, d_1) Cross-sectional morphology of the heterojunction. (e, e_1) HRTEM image and electron diffraction pattern along [2, -1, -1, 0] axis of the sapphire substrate. (f, f1) HRTEM image and electron diffraction pattern along [0, 1, 0] axis of the $(Al_{0.68}Ga_{0.32})_2O_3$ film. (g) SIMS of Si and Ga elements in the Ga_2O_3:Si film.

occupies the position of gallium ion in the original gallium oxide lattice in a trivalent form [31]. In addition, the atomic ratio of Al/Ga element (~68/32) is obtained by calculating their XPS peak areas. When the etching proceeds (6100 s < t < 7200 s), the Al/Ga atomic ratio gradually increases, which is attributed to the transition from gallium oxide layer to aluminum oxide layer. By controlling the growth time of Ga_2O_3:Si layer with a growth speed of 130 nm h^{-1}, the thickness of the conductive Ga_2O_3:Si film is speculated to be around 10 nm. The transmittance spectrum of Ga_2O_3:Si can be found in Fig. S3. Fig. 3e characterizes the position of valence band in $(Al_{0.68}Ga_{0.32})_2O_3$ film, which is about 3.46 eV from the Fermi level. At the same time, XPS was further used to study the inelastic energy loss in the atomic spectrum of O 1s core level of the thin film (Fig. 3f). In this way, the bandgap of $(Al_{0.68}Ga_{0.32})_2O_3$ is determined to be approximately 6.1 eV [36]. According to abovementioned results, it can be inferred that $(Al_{0.68}Ga_{0.32})_2O_3$ film is in the intrinsic state of high resistance based on the bandgap and the position of Fermi level.

Based on the $(Al_{0.68}Ga_{0.32})_2O_3/Ga_2O_3$:Si epitaxial film, a full gallium oxide heterostructure VUV detector was fabricated. The schematic diagram of device prototype is shown in Fig. 4a, in which an ultrathin Pt layer (20 nm) was deposited on the $(Al_{0.68}Ga_{0.32})_2O_3$ surface as top electrodes. The Pt electrodes have a high transmittance up to 70% in the VUV region (Fig. 4b). The thin layer electrodes can reduce the optical energy loss of incident VUV radiation due to the absorption or reflection of the commonly used electrode materials, whereby it will increase the utilization efficiency of incident light [7]. *I-V* characteristic curves of the detector in the dark and under 185-nm illumination are drawn in Fig. 4c. With an ul-

 © Science China Press and Springer-Verlag GmbH Germany, part of Springer Nature 2021

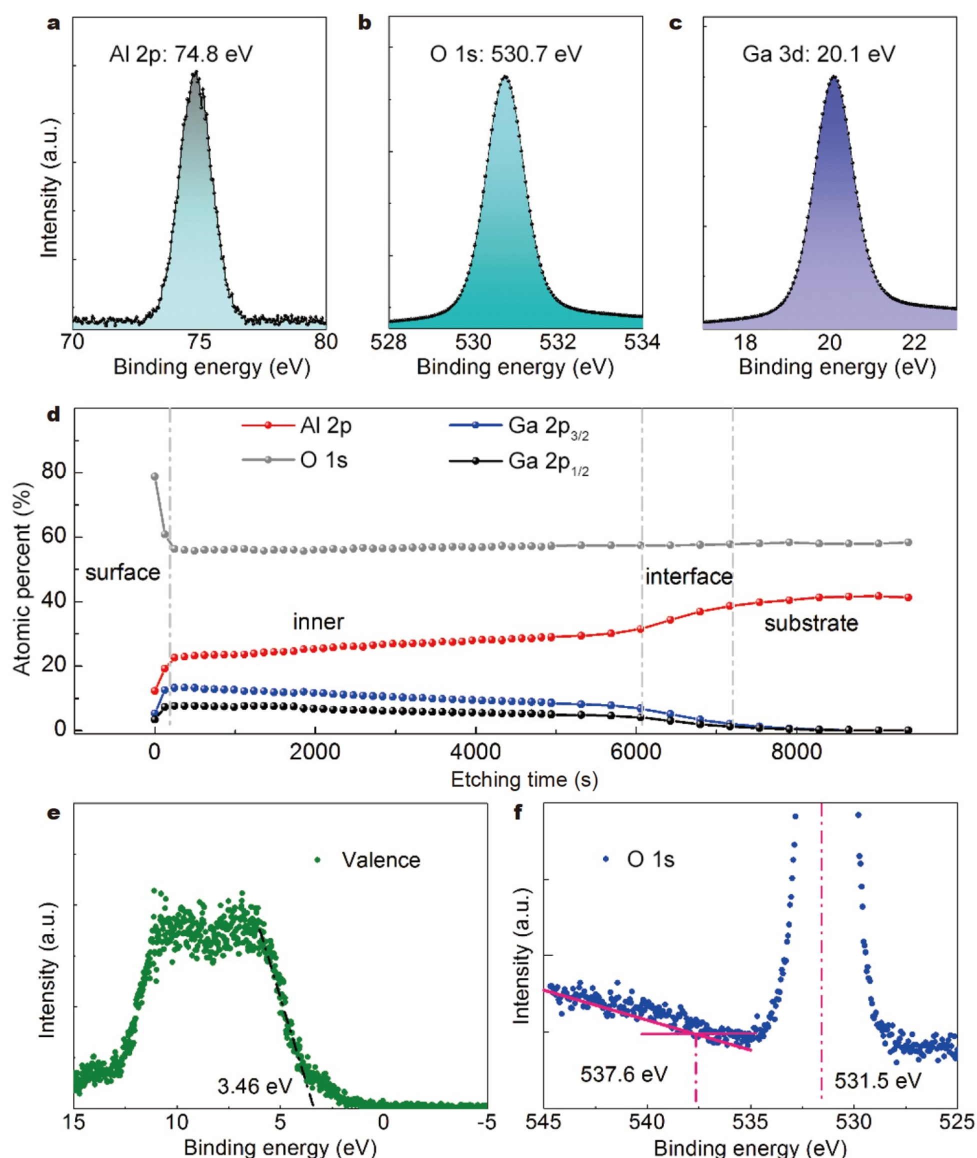

Figure 3 XPS characterizations of the film. (a–c) High-resolution XPS peaks of Al 2p, O 1s and Ga 3d in $(Al_{0.68}Ga_{0.32})_2O_3$ film. (d) Dependence of atomic percent (Al, O and Ga) on etching time. The atomic percentage of element O is observed to stay at around 57%. (e) Ga $2p_{3/2}$ valence band maximum of $(Al_{0.68}Ga_{0.32})_2O_3$ thin film. (f) O 1s core-level binding energy spectrum and the energy loss structure of $(Al_{0.68}Ga_{0.32})_2O_3$ thin film, where the estimated bandgap is shown.

trahigh switching ratio of three orders of magnitude and an open-circuit voltage of 1.0 V, this device is a typical photovoltaic detector. Fig. 4d shows the device's spectral response at −10 V bias. Near the wavelength of 198 nm, this device has a responsivity of ~86 mA W^{-1}, which means that the detector has a high sensitivity to VUV light and possesses the spectral selective detection ability. The corresponding external quantum efficiency (EQE) values depending on the incident wavelength are plotted in Fig. S4.

Multi-cycle time-dependent photoresponse at 0 V bias indicates that the photoelectric performance of this device is repeatable (Fig. 5a). By analyzing the rising and falling edges of one single photoresponse (Fig. 5b), a rise time of 1.2 s and a decay time of 0.2 s are observed, respectively. Here, the rise time is defined as the time taken for the photocurrent to rise to 90% of its maximum value, and the fall time is defined in a similar way [41,42]. The multi-cycle time-dependent photoresponses of this device at different bias voltages are shown in Fig. 5c. As the bias

 © Science China Press and Springer-Verlag GmbH Germany, part of Springer Nature 2021

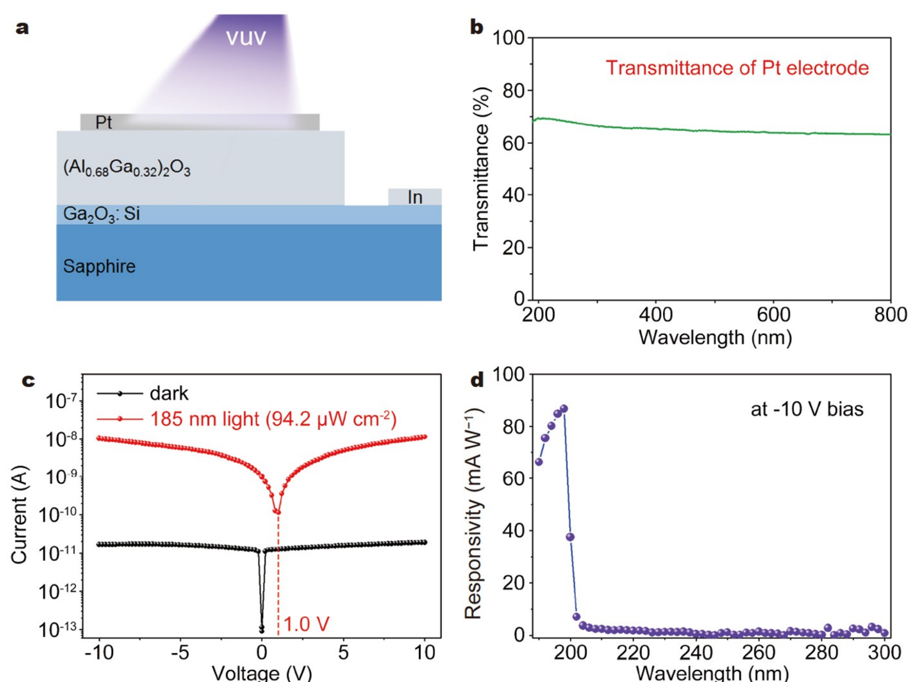

Figure 4 Detector schematic and its optoelectronic properties. (a) Schematic diagram of the $(Al_{0.68}Ga_{0.32})_2O_3/Ga_2O_3$:Si/sapphire photodetector. The radius of the round platinum electrode is 200 μm, and the thickness of it is around 20 nm. (b) The UV-visible transmittance of Pt electrodes. (c) *I-V* characteristics of the photodetector in the dark and under 185-nm light with 94.2 μW cm^{-2} at room temperature. (d) Spectrum responsivity of the photodetector measured at the −10 V bias voltage.

voltage increases, the photocurrent also increases, which is due to that the applied bias voltage enhances the photogenerated carrier separation efficiency [43]. The relationship between the detector's speed and external bias voltage shows (Fig. 5d) that the switching time almost does not change with bias voltages and stably stays within a small range. However, the rise time is slightly increased at 0 V bias, indicating a weak auxiliary influence on carrier transport from the external electric field. Increasing the strength of external electric field cannot continuously improve the response speed, which complies with the characteristics of photovoltaic devices [25,44].

The detector's photoelectric characteristics under different illumination intensities of 185-nm light are shown in Fig. 6, where the photocurrent increases at both forward and reverse bias as the light intensity increases (Fig. 6a). Based on the meticulous analysis of the dependence of photocurrent and open-circuit voltage *versus* illumination intensity, it is found that the photocurrent increases linearly with the VUV light power density (Fig. 6b) at 0 V bias, which indicates the good linear response characteristic of the photovoltaic detector. On the contrary, the open-circuit voltage tends to be saturated, which is attributed to the absorption saturation of incident photons in the $(Al_{0.68}Ga_{0.32})_2O_3$ film, consistent with the previous reports [18]. The responsivity hardly depends on the change of light power, exhibiting the stable output characteristics. According to the EQE calculation formula [20]: EQE=$(Rhc)/(e\lambda)$, where R is the responsivity, h the Planck constant, c the speed of light, e the charge of electron and λ the wavelength of incident light. Under an illumination of 185-nm light with 94.2 μW cm^{-2}, it is calculated that the photovoltaic VUV detector has an EQE of 5.5% at the bias voltage of 0 V. As the applied bias voltage increases to −5 V, the EQE increases to 33.4% (Fig. 6d).

The performance of currently-reported detectors based on $(AlGa)_2O_3$ ternary oxide films with different percentages of Al contents is also compared, as shown in Table 1. Compared with that of binary oxide Ga_2O_3 detectors, the response peak of the ternary oxide $(AlGa)_2O_3$ detector is much shorter, and shifts to 198 nm in this work, realizing the selective response to VUV band of gallium oxide-based detectors [27–29]. In addition, this device also has a dark current as low as 1.6×10^{-11} A and displays typical photovoltaic characteristics. All these results demonstrate a potential application of ternary oxides

 © Science China Press and Springer-Verlag GmbH Germany, part of Springer Nature 2021

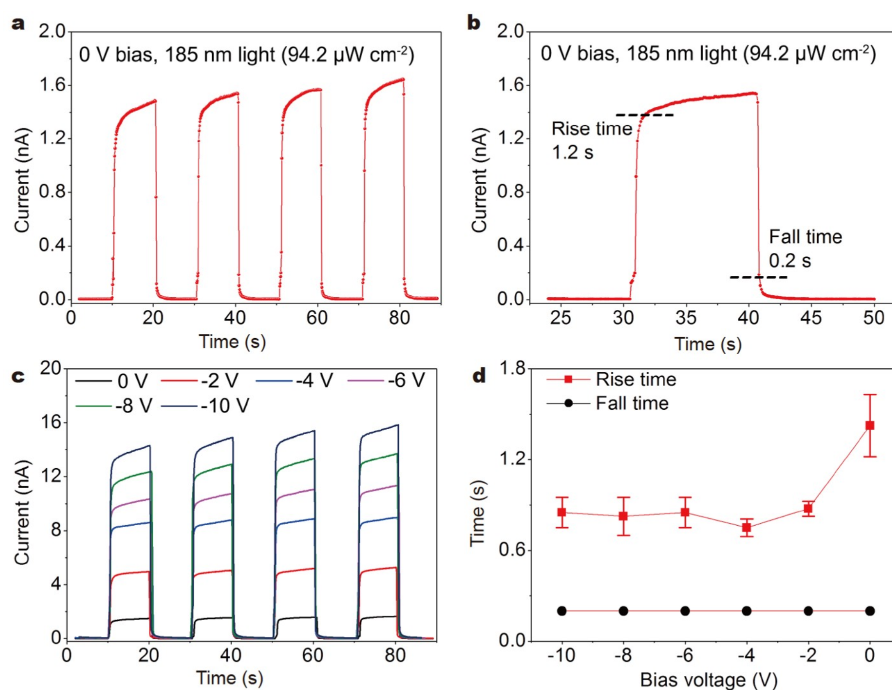

Figure 5 Time-dependent photoresponse of the detector at a series of bias voltages. (a) Multi-cycle time-dependent photoresponse of the detector at 0 V and under 185 nm illumination with 94.2 μW cm^{-2}. (b) Enlarged view of a single time-dependent photoresponse. (c) Multi-cycle time-dependent photoresponses under various bias voltages from 0 to −10 V, and the light intensity is 94.2 μW cm^{-2}. The photocurrent has been taken as absolute values. (d) The dependences of rise and fall times on bias voltages.

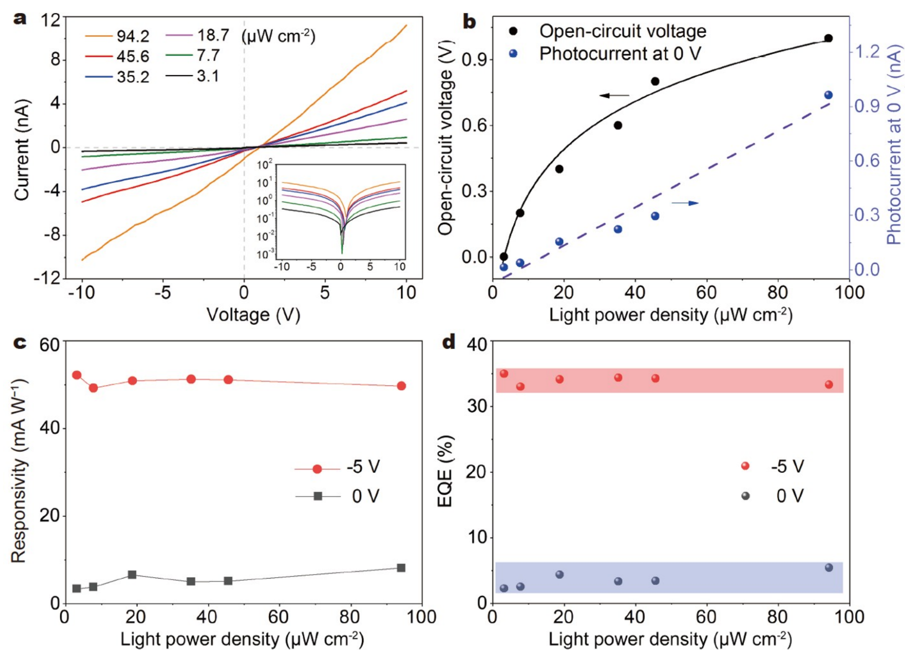

Figure 6 Dependence of the detector on light intensity. (a) *I-V* characteristics of the photodetector under 185-nm light with the ranging illumination intensity from 3.1 to 94.2 μW cm^{-2}. The inset plots the *I-V* curves in the log form. (b) Dependence of photocurrent at 0 V and open-circuit voltage *versus* light intensity. (c, d) Responsivity and EQE vary with the light intensity at 0 and −5 V, respectively.

 © Science China Press and Springer-Verlag GmbH Germany, part of Springer Nature 2021

Table 1 Performance comparison of different photodetectors based on $(AlGa)_2O_3$ film

Materials	Type	Responsivity ($A\ W^{-1}$)	Dark current (A)	Response peak (nm)	Refs.
$(Al_{0.14}Ga_{0.86})_2O_3$	Photoconductive	1.38@5 V	9.6×10^{-13}	230	[27]
$(Al_{0.35}Ga_{0.65})_2O_3$	Photoconductive	0.60@20 V	–	238	[28]
$(Al_{0.35}Ga_{0.65})_2O_3$	Photoconductive	0.0025@−20 V	0.44×10^{-12}	230	[29]
Gr./$(Al_{0.18}Ga_{0.82})_2O_3$/GaN	Photovoltaic	0.02@0 V	–	210	[30]
$(Al_{0.68}Ga_{0.32})_2O_3/Ga_2O_3$:Si	Photovoltaic	0.086@−10 V 0.0081@0 V	1.6×10^{-11}	198	This work

doped with high Al contents in the field of VUV detection.

CONCLUSION

Conductive Ga_2O_3:Si layer and ternary oxide $(Al_{0.68}Ga_{0.32})_2O_3$ film are sequentially grown on the sapphire substrate by using the MOCVD method. Based on the $(Al_{0.68}Ga_{0.32})_2O_3/Ga_2O_3$:Si composite film, a VUV photovoltaic detector with low dark current (1.6×10^{-11} A) and high responsivity (8.1 mA W^{-1}@0V) is fabricated. The excellent performance of this detector can be partially attributed to the insertion of conductive Ga_2O_3:Si layer. Benefiting from the ultrathin film, the lattice mismatch between the $(Al_{0.68}Ga_{0.32})_2O_3$ photosensitive layer and sapphire substrates is almost unchanged, ensuring a high crystalline quality of the ternary sesquioxides even in the case of high Al content (~68%). In addition, the built-in electric field constructed between $(Al_{0.68}Ga_{0.32})_2O_3$ and Ga_2O_3:Si layer enables the device to work stably at 0 V bias. The utilization of Ga_2O_3:Si conductive layer not only improves the performance of detectors, but also gives an inspiration to adjust the bandgap of other sesquioxides.

Received 28 February 2021; accepted 30 April 2021; published online 7 July 2021

1 Zheng W, Jia L, Huang F. Vacuum-ultraviolet photon detections. iScience, 2020, 23: 101145
2 Zheng W, Huang F, Zheng R, *et al.* Low-dimensional structure vacuum-ultraviolet-sensitive (λ<200 nm) photodetector with fast-response speed based on high-quality AlN micro/nanowire. Adv Mater, 2015, 27: 3921–3927
3 Zheng W, Lin R, Jia L, *et al.* Vacuum ultraviolet photovoltaic arrays. Photon Res, 2019, 7: 98–102
4 Zheng W, Lin R, Zhang D, *et al.* Vacuum-ultraviolet photovoltaic detector with improved response speed and responsivity *via* heating annihilation trap state mechanism. Adv Opt Mater, 2018, 6: 1800697
5 Jia L, Zheng W, Huang F. Vacuum-ultraviolet photodetectors. PhotoniX, 2020, 1: 22
6 Monroy E, Omn s F, Calle F. Wide-bandgap semiconductor ultraviolet photodetectors. Semicond Sci Technol, 2003, 18: R33–R51
7 Li Y, Zheng W, Huang F. All-silicon photovoltaic detectors with deep ultraviolet selectivity. PhotoniX, 2020, 1: 15
8 Lin R, Zheng W, Zhang D, *et al.* Brushed crystallized ultrathin oxides: Recrystallization and deep-ultraviolet imaging application. ACS Appl Electron Mater, 2019, 1: 2166–2173
9 Xu J, Zheng W, Huang F. Gallium oxide solar-blind ultraviolet photodetectors: A review. J Mater Chem C, 2019, 7: 8753–8770
10 Peng L, Hu L, Fang X. Low-dimensional nanostructure ultraviolet photodetectors. Adv Mater, 2013, 25: 5321–5328
11 Kong WY, Wu GA, Wang KY, *et al.* Graphene-β-Ga_2O_3 heterojunction for highly sensitive deep UV photodetector application. Adv Mater, 2016, 28: 10725–10731
12 Zheng W, Lin R, Ran J, *et al.* Vacuum-ultraviolet photovoltaic detector. ACS Nano, 2018, 12: 425–431
13 Li T, Wang F, Lin R, *et al.* In-plane enhanced epitaxy for step-flow AlN yielding a high-performance vacuum-ultraviolet photovoltaic detector. CrystEngComm, 2020, 22: 654–659
14 Jia L, Zheng W, Lin R, *et al.* Ultra-high photovoltage (2.45 V) forming in graphene heterojunction via quasi-fermi level splitting enhanced effect. iScience, 2020, 23: 100818
15 Sun H, Mitra S, Subedi RC, *et al.* Unambiguously enhanced ultraviolet luminescence of AlGaN wavy quantum well structures grown on large misoriented sapphire substrate. Adv Funct Mater, 2019, 29: 1905445
16 Huang C, Zhang H, Sun H. Ultraviolet optoelectronic devices based on AlGaN-SiC platform: Towards monolithic photonics integration system. Nano Energy, 2020, 77: 105149
17 Wang D, Liu X, Fang S, *et al.* Pt/AlGaN nanoarchitecture: Toward high responsivity, self-powered ultraviolet-sensitive photodetection. Nano Lett, 2021, 21: 120–129
18 Zheng W, Lin R, Jia L, *et al.* Vacuum-ultraviolet-oriented van der Waals photovoltaics. ACS Photonics, 2019, 6: 1869–1875
19 Caldwell JD, Aharonovich I, Cassabois G, *et al.* Photonics with hexagonal boron nitride. Nat Rev Mater, 2019, 4: 552–567
20 Zheng W, Lin R, Zhang Z, *et al.* Vacuum-ultraviolet photodetection in few-layered h-BN. ACS Appl Mater Interfaces, 2018, 10: 27116–27123
21 Dahal R, Li J, Majety S, *et al.* Epitaxially grown semiconducting hexagonal boron nitride as a deep ultraviolet photonic material. Appl Phys Lett, 2011, 98: 211110
22 Li Y, Guo J, Zheng W, *et al.* Amorphous boron nitride for vacuum-ultraviolet photodetection. Appl Phys Lett, 2020, 117: 023504
23 Guo D, Wu Z, Li P, *et al.* Fabrication of β-Ga_2O_3 thin films and solar-blind photodetectors by laser MBE technology. Opt Mater Express, 2014, 4: 1067–1076
24 Zhang Q, Jie J, Diao S, *et al.* Solution-processed graphene quantum dot deep-UV photodetectors. ACS Nano, 2015, 9: 1561–1570
25 Ai M, Guo D, Qu Y, *et al.* Fast-response solar-blind ultraviolet photodetector with a graphene/β-Ga_2O_3/graphene hybrid struc-

 © Science China Press and Springer-Verlag GmbH Germany, part of Springer Nature 2021

ture. J Alloys Compd, 2017, 692: 634–638
26 Lin R, Zheng W, Zhang D, *et al.* High-performance graphene/β-Ga_2O_3 heterojunction deep-ultraviolet photodetector with hot-electron excited carrier multiplication. ACS Appl Mater Interfaces, 2018, 10: 22419–22426
27 Yuan SH, Wang CC, Huang SY, *et al.* Improved responsivity drop from 250 to 200 nm in sputtered gallium oxide photodetectors by incorporating trace aluminum. IEEE Electron Device Lett, 2018, 39: 220–223
28 Feng Q, Li X, Han G, *et al.* $(AlGa)_2O_3$ solar-blind photodetectors on sapphire with wider bandgap and improved responsivity. Opt Mater Express, 2017, 7: 1240–1248
29 Liao C H, Badan Y, Da Prato G, *et al.* β-$(AlGa)_2O_3$ solar-blind photodetector fabricated by high-temperature driven interdiffusion method (Conference Presentation). SPIE OPTO, San Francisco, 2020, doi: 10.1117/12.2544676
30 Zhang D, Lin W, Liu S, *et al.* Ultra-robust deep-UV photovoltaic detector based on graphene/$(AlGa)_2O_3$/GaN with high-performance in temperature fluctuations. ACS Appl Mater Interfaces, 2019, 11: 48071–48078
31 Zhang D, Zheng W, Lin R, *et al.* Ultrahigh EQE (15%) solar-blind UV photovoltaic detector with organic-inorganic heterojunction *via* dual built-in fields enhanced photogenerated carrier separation efficiency mechanism. Adv Funct Mater, 2019, 29: 1900935
32 Zhang H, Huang C, Song K, *et al.* Compositionally graded III-nitride alloys: Building blocks for efficient ultraviolet optoelectronics and power electronics. Reports on progress in physics Physical Society (Great Britain), 2021
33 Zhang D, Zheng W, Lin RC, *et al.* High quality β-Ga_2O_3 film grown with N_2O for high sensitivity solar-blind-ultraviolet photodetector with fast response speed. J Alloys Compd, 2018, 735: 150–154
34 Nakagomi S, Kokubun Y. Crystal orientation of β-Ga_2O_3 thin films formed on c-plane and a-plane sapphire substrate. J Cryst Growth, 2012, 349: 12–18
35 Kumar S, Sarau G, Tessarek C, *et al.* Study of iron-catalysed growth of β-Ga_2O_3 nanowires and their detailed characterization using TEM, Raman and cathodoluminescence techniques. J Phys D-Appl Phys, 2014, 47: 435101
36 Kamimura T, Sasaki K, Hoi Wong M, *et al.* Band alignment and electrical properties of Al_2O_3/β-Ga_2O_3 heterojunctions. Appl Phys Lett, 2014, 104: 192104
37 Gottschalch V, Mergenthaler K, Wagner G, *et al.* Growth of β-Ga_2O_3 on Al_2O_3 and GaAs using metal-organic vapor-phase epitaxy. Phys Status Solidi A, 2009, 206: 243–249
38 Lee WE, Lagerlof KPD. Structural and electron diffraction data for sapphire (α-Al_2O_3). J Elec Microsc Tech, 1985, 2: 247–258
39 Jiang ZX, Wu ZY, Ma CC, *et al.* P-type β-Ga_2O_3 metal-semiconductor-metal solar-blind photodetectors with extremely high responsivity and gain-bandwidth product. Mater Today Phys, 2020, 14: 100226
40 Wu ZY, Jiang ZX, Ma CC, *et al.* Energy-driven multi-step structural phase transition mechanism to achieve high-quality p-type nitrogen-doped β-Ga_2O_3 films. Mater Today Phys, 2021, 17: 100356
41 Dong H, Long S, Sun H, *et al.* Fast switching β-Ga_2O_3 power MOSFET with a trench-gate structure. IEEE Electron Device Lett, 2019, 40: 1385–1388
42 Hou X, Sun H, Long S, *et al.* Ultrahigh-performance solar-blind photodetector based on α-phase-dominated Ga_2O_3 film with record low dark current of 81 fA. IEEE Electron Device Lett, 2019, 40: 1483–1486
43 Li Y, Zhang D, Lin R, *et al.* Graphene interdigital electrodes for improving sensitivity in a Ga_2O_3:Zn deep-ultraviolet photoconductive detector. ACS Appl Mater Interfaces, 2019, 11: 1013–1020
44 Xu C, Du Z, Huang Y, *et al.* Amorphous-MgGaO film combined with graphene for vacuum-ultraviolet photovoltaic detector. ACS Appl Mater Interfaces, 2018, 10: 42681–42687

Acknowledgements This work was supported by the National Natural Science Foundation of China (91833301 and 61427901), Guangdong Natural Science Funds for Distinguished Young Scholars (2021B1515020105), and Guangdong Basic and Applied Basic Research Foundation (2019A1515110916).

Author contributions Li Y, Zhang D and Jia L performed the experiments; Li Y analyzed the data and wrote the paper with support from Zhang D and Zheng W. All authors contributed to the general discussion.

Conflict of interest The authors declare no conflict of interest.

Supplementary information Supporting information, including XRD characterization of $(AlGa)_2O_3$ and Ga_2O_3:Si, HRTEM images of the materials, external quantum efficiency of the photodetector, UV-Vis transmission spectra of sapphire and Ga_2O_3:Si film, is available in the online version of the paper.

Yuqiang Li obtained his bachelor's degree from Sun Yat-sen University in 2016. He is a PhD candidate at the School of Materials, Sun Yat-sen University. His research interest focuses on wide-bandgap semiconductor materials and devices.

Dan Zhang graduated from the University of the Chinese Academy of Sciences with a doctorate degree in 2017. She is now an associate researcher at the School of Materials, Sun Yat-sen University. Her main research field is wide-bandgap semiconductor materials and devices.

Wei Zheng received his PhD degree from Shenzhen University in 2014. His research interest focuses on semiconductor-based vacuum-ultraviolet (10–200 nm) photodetectors and condensed matter physics in ultra-wide bandgap semiconductors.

 © Science China Press and Springer-Verlag GmbH Germany, part of Springer Nature 2021

以晶格匹配策略设计的超宽禁带(6.14 eV) $(AlGa)_2O_3/Ga_2O_3$异质结用于高灵敏度真空紫外探测

李宇强, 张丹*, 贾乐敏, 朱思琪, 朱燕明, 郑伟*, 黄丰

摘要 本文展示了一种利用超薄导电的Ga_2O_3:Si纳米层获得$(AlGa)_2O_3$结晶薄膜的设计策略．受益于Ga_2O_3:Si插层的存在，高质量的$(Al_{0.68}Ga_{0.32})_2O_3$倍半氧化物薄膜得以在蓝宝石衬底上外延生长，其中铝组分含量高达~68%，并被多种技术如HRTEM，XPS和XRD等进行了系统性表征．$(Al_{0.68}Ga_{0.32})_2O_3$材料的带隙被成功拓宽至6.14 eV，我们在此基础上制备出了$(AlGa)_2O_3/Ga_2O_3$:Si真空紫外光电探测器．该探测器性能优异，开关比高达10^3，开路电压为1.0 V, 0 V偏压下响应度为8.1 mA W^{-1}. 以上结果表明, 本文提出的生长策略可有效提高$(AlGa)_2O_3$倍半氧化物的质量并调节其带隙，有助于推动其在真空紫外探测领域的实际应用.

 © Science China Press and Springer-Verlag GmbH Germany, part of Springer Nature 2021